

Gravity-Aware Monocular 3D Human-Object Reconstruction

Rishabh Dabral^{1,2} Soshi Shimada² Arjun Jain^{3,4} Christian Theobalt² Vladislav Golyanik²
¹IIT Bombay ²MPI for Informatics, SIC ³IISc Bangalore ⁴Fast Code AI

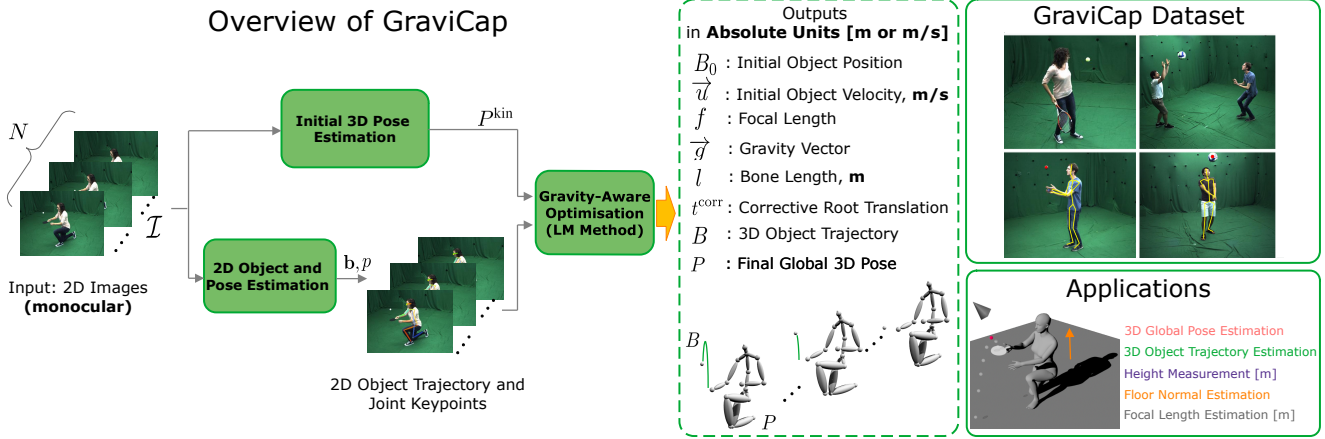


Figure 1. The proposed GRAVICAP approach captures 3D human motions and 3D object trajectories from monocular RGB videos. (Left:) Thanks to the physics-based constraints, we can disambiguate the scene’s scale in the monocular setting and recover 3D human poses and the trajectories in meters. (Right:) We evaluate our method on a new real multi-view dataset with several subjects and activities.

Abstract

This paper proposes GraviCap, i.e., a new approach for joint markerless 3D human motion capture and object trajectory estimation from monocular RGB videos. We focus on scenes with objects partially observed during a free flight. In contrast to existing monocular methods, we can recover scale, object trajectories as well as human bone lengths in meters and the ground plane’s orientation, thanks to the awareness of the gravity constraining object motions. Our objective function is parametrised by the object’s initial velocity and position, gravity direction and focal length, and jointly optimised for one or several free flight episodes. The proposed human-object interaction constraints ensure geometric consistency of the 3D reconstructions and improved physical plausibility of human poses compared to the unconstrained case. We evaluate GraviCap on a new dataset with ground-truth annotations for persons and different objects undergoing free flights. In the experiments, our approach achieves state-of-the-art accuracy in 3D human motion capture on various metrics. We urge the reader to watch our supplementary video. Both the source code and the dataset are released; see <http://4dqv.mpi-inf.mpg.de/GraviCap/>.

1. Introduction

Markerless 3D human motion capture from a single monocular RGB camera has many open challenges. Although state-of-the-art methods have seen great progress [21, 24, 33, 14, 39], they still hardly work for scenes showing non-trivial interactions of humans with the environment as most of them do not model environmental constraints or physical laws. Further, 3D reconstruction of humans interacting with objects from monocular imagery is scarcely explored, and only a few works were proposed to date [19, 50]. Most existing methods that consider interaction with the environment impose geometric constraints to avoid incorrect interpenetrations [49, 15, 50]. They often exhibit strong jitter, implausible posture with unnatural body leaning and depth instabilities. Recent physics-based methods for monocular 3D human pose estimation [34, 39] showed that explicit modelling of gravity and ground reaction forces (or friction) enables monocular reconstruction of humans of much higher biomechanical plausibility. However, these methods do not model object interactions, and without a priori information about the human body, they cannot estimate posture and scene dimensions in absolute metric scale.

In this paper, we make the following observation: Explicitly modelling physics and actively encouraging a spe-

cific form of human-object interaction in the scene *enables improved 3D human and 3D object trajectory reconstruction in a metrically accurate way from a single monocular video*. We consider scenarios when up to two persons are interacting with an object and bringing it to a free flight (*e.g.*, throwing or tossing). Such scenarios are often observed in real everyday life while practising sports or playing outdoor games. We show that physics-based constraints allow us to obtain 3D estimates in the absolute units, which, otherwise, remains inaccessible for a monocular setting when no strong prior assumptions about the scene can be made, such as known bone lengths.

Our core findings are that 1) Projectile motion constraints are sufficient to recover the 3D trajectory of an object undergoing free flight from 2D object coordinates, assuming known camera frame rate and gravity vector; 2) Knowing the magnitude of the gravity and the focal length is sufficient to resolve the scale of the observed scene in meters and orientation of the ground plane, assuming that the direction of the gravity vector is opposite to the ground plane normal; 3) Localising humans with respect to the recovered 3D object trajectory leads to improved 3D human motion capture. See Fig. 1 for an overview of our framework. The inputs are 2D coordinates of the object’s geometric centre and 2D human joint locations, along with initial unconstrained kinematic 3D human poses. After that, we then minimise the proposed objective globally over multiple input frames and obtain 3D object trajectory over one or several free-flight episodes and improved 3D human poses. Summarised, the **contributions** of this work are as follows:

- GRAVICAP, *i.e.*, the new approach for joint 3D capture of human motions and trajectories of objects undergoing free flights (Sec. 3);
- New types of human-object interaction constraints improving the accuracy and physical plausibility of 3D human poses (Sec. 3.2.2). For the first time, these constraints allow recovering camera-relative distances of moving and interacting objects, including humans, in meters from a single monocular RGB camera;
- A new dataset of human-object interactions for experimental evaluation, with ground-truth annotations of 3D human poses and object trajectories (Sec. 4).

We achieve state-of-the-art accuracy for global 3D human motion capture using different metrics in extensive experiments with the new dataset (Sec. 5). Our estimates look more physically plausible and temporally consistent compared to results without human-trajectory localisation constraints. Moreover, the proposed constraints significantly improve absolute root translations. The source code of GRAVICAP and the dataset are publicly available at <http://4dqv.mpi-inf.mpg.de/GraviCap/>.

2. Related Work

Kinematic 3D Human Pose Estimation. The accuracy of monocular 3D human pose estimation significantly progressed during recent years. Most methods employ neural networks and can be classified into several categories. Some methods first estimate 2D poses in the input views and then lift them in the 3D space [6, 21, 41, 27, 11, 8], whereas several others estimate 3D joints directly from the images [40, 22, 35]. Several lifting algorithms build upon the principles of non-rigid structure from motion and rely on classical optimisation for the lifting step [51, 45, 18]. At the same time, weakly-supervised methods gain more and more attention, due to improved generalisability beyond the training datasets [9, 46, 7, 30]. Many other approaches combine regression of 2D joint locations or 3D joint depths [29, 24, 31, 14]. Parametric body models provide strong priors on plausible shapes and poses, which can be leveraged for accurate human pose estimation [4, 16, 32, 17]. Even a stronger prior is a human mesh, and several recent methods show how to use it for tracking a single actor [13, 12, 48]. In contrast to all approaches discussed so far, several other techniques generalise to scenarios with multiple subjects [8, 36, 26, 23]. Several purely kinematic methods attempt to estimate 3D human poses with absolute depths in the camera coordinate space [26, 37, 23]. All approaches reviewed so far consider geometric fidelity of the reconstructed motions and do not impose environmental constraints.

3D Human Pose Estimation with Environmental Priors. Hassan *et al.* [15] use 3D environmental scans to detect human-object collisions and improve kinematic 3D pose regression. Environmental constraints such as a common ground plane and volume occupancy exclusions are effectively applied in Zanfir *et al.* [49] for 3D human pose and shape estimation. Zhang *et al.* [50] jointly reconstruct humans and objects relying on geometric shape priors, both for humans and objects, as well as interactional vicinity. iMapper of Monszpart and colleagues [25] jointly recovers schematic 3D scene arrangements and human motions in a data-driven manner, relying on a database of 3D human-object interactions for training. The authors show that motion patterns provide a strong cue about scene compositions, which, in turn, serve as priors for possible human motions. Similarly, we find in this paper that the physics-based cues associated with the object’s motion caused by the gravitation can better constrain human poses.

Vondrak *et al.* [44] capture 3D human motions by recovering 3D bipedal controllers that simulate motions observed in the videos. Li *et al.* [19] simultaneously estimate 3D trajectories of human skeletal joints and an instrument (used by the person), as well as forces at contact positions (*i.e.*, foot-floor and hand-object contacts). They observe that the instrument provides a reconstruction cue for hands in 3D (*i.e.*, for their relative positioning in depth), and the hand

positions provide a cue for the instrument’s 3D position. In contrast, we focus on objects that can be released and move freely under gravity along a ballistic trajectory. Three recent methods constrain human motions with bio-physical plausibility constraints [34, 39, 38]. This allows significantly reducing unnatural body leaning, foot-floor penetration and jitter. We formulate physics-based constraints for objects and not directly humans. In contrast to all reviewed methods using environmental priors, we can disambiguate the scale of the scene and calculate the distances (e.g., bone lengths and 3D object trajectories) in meters. Moreover, 3D human poses estimated this way are more physically-plausible compared to the initial kinematic estimates, thanks to our human-object localisation constraints.

Other Related Problems. As a side effect, our GRAVICAP can extract absolute bone lengths from monocular videos. Several methods extract anthropometric measurements using 3D registration techniques and assume 3D human body scans as inputs [42, 47], whereas we rely on 2D video inputs only. Bieler *et al.* [3] use equations of classical mechanics for estimation of human height from videos of jumping people. We can estimate human height as a by-product of scale disambiguation and due to the reconstructed object motion.

Bhat *et al.* [2] show how to estimate rigid body’s motion in free flight with a simulation that agrees with the image observations. Assuming a known shape of a small order of rotational symmetry allows estimating the initial position and velocity of the object, gravity direction and extrinsic parameters of the object relative to the camera. In contrast, we assume that 1) The target objects have infinite order of rotational symmetry (i.e., they are spherical) and 2) Their diameter is unknown. We show that these assumptions are sufficient to disambiguate the scene’s scale.

3. Approach

We now describe our GRAVICAP approach for jointly recovering the object and human trajectories in the camera’s frame of reference; see Fig. 1 for an overview.

3.1. Recovering the 3D Object Trajectory

First, we assume known camera focal length f and a set of 2D observations of an object’s ballistic trajectory $\mathbf{b} = \{b_1, b_2, \dots, b_N\}$ extracted from images $\mathcal{I} = \{\mathcal{I}_1, \mathcal{I}_2, \dots, \mathcal{I}_N\}$, where $b_i = (x_i, y_i)$ is the object’s position in image $i \in \{1, \dots, N\}$. Our goal is to recover the object’s 3D trajectory $B = \{B_1, B_2, \dots, B_N\}$, where $B_i = (X_i, Y_i, Z_i)$ represents the object’s position in the camera-relative 3D space. We call *episode* one free flight event observed in a monocular video. We assume that once released, the only force influencing the motion of the object is gravity (there is no air resistance). This assumption allows us to parameterise B using three parameters: The initial velocity $\vec{u} = (u_x, u_y, u_z)$, the object’s initial position

B_0 and the gravity vector $\vec{g} = (g_x, g_y, g_z)$ as viewed in the camera’s frame of reference. Given frame rate r , B can be expressed using the equations of Newtonian dynamics as

$$B_i = B_0 + \vec{u}t + \frac{1}{2}\vec{g}t^2, \quad (1)$$

where $t = i/r$ is the time stamp in seconds corresponding to the frame i from the beginning of the free flight.

Next, assuming intrinsic camera parameters (focal length f and principal point $c = (c_x, c_y)$) and gravity vector \vec{g} are known, it is possible to reconstruct the 3D trajectory B of the object from 2D observations \mathbf{b} . Under the pinhole camera model, the observed object’s trajectory in the video can be explained as follows:

$$\begin{aligned} x_i &= f \frac{X_i}{Z_i} + c_x, \quad y_i = f \frac{Y_i}{Z_i} + c_y, \quad \forall i, \\ \text{s. t. } &\sqrt{g_x^2 + g_y^2 + g_z^2} = 9.81 \text{ m/s}^2, \end{aligned} \quad (2)$$

$$\text{where } \begin{cases} X_i = X_0 + u_x t + \frac{1}{2}g_x t^2, \\ Y_i = Y_0 + u_y t + \frac{1}{2}g_y t^2, \quad \text{and} \\ Z_i = Z_0 + u_z t + \frac{1}{2}g_z t^2. \end{cases} \quad (3)$$

The equation system (2) has $3N$ unknowns. Using the parametrisation with the ballistic trajectories (3), it reduces to six, i.e., three for the initial position $B_0 = (X_0, Y_0, Z_0)$ and three for \vec{u} . Thus, (2) has a unique solution when $N > 2$ (for $N=3$, it has a closed-form solution).

We next consider two cases, i.e., when the direction of \vec{g} is 1) known and when it is 2) unknown in (2). In the first case, we assume that the direction of \vec{g} is parallel to the y -axis and coincides with the flipped floor normal in the world coordinate system. This is highly relevant in practice, especially in artificial environments. In the second case, the orientation of the ground plane with respect to the camera remains unknown. Consequently, (2) contains three more unknowns and has a solution if $N > 4$.

At the same time, in both cases we assume that the magnitude of \vec{g} is known and equals 9.81 m/s^2 , which is a reasonable assumption. Even though \vec{g} differs depending on the location on Earth, the differences are insignificant and lie beyond the values which can improve the attainable precision in the 3D trajectory estimation from monocular images in our setting¹. If both f and \vec{g} are unknown, (2) has ten unknowns which can be recovered with $N > 5$, subject to proper initialisation (see comments on the ‘ f/Z ’ ambiguity in Sec. 6). In practice, we use and recommend $N > 10$ to obtain a better determined system (compared to $N=5$). A solution to such a system is less sensitive to noise in the 2D measurements and quantisation effects. Table 1 summarises

¹ $\|\vec{g}\| = 9.81 \text{ m/s}^2$ is close to the mean value of $\|\vec{g}\|$ on the surface of Earth, and $\|\vec{g}\|$ differs not more than by $\approx 0.7\%$ across locations.

mode / recovery of . . .	inputs	unknowns
3D object coordinates, scene scale (6 DoF)	\mathbf{b}, \vec{g}, f	\vec{u}, B_0
+gravity direction (9 DoF)	$\mathbf{b}, \ \vec{g}\ , f$	\vec{u}, B_0, \vec{g}
+focal length (10 DoF)	$\mathbf{b}, \ \vec{g}\ $	\vec{u}, B_0, f, \vec{g}
6 DoF + f (7 DoF)	\mathbf{b}, \vec{g}	\vec{u}, B_0, f

Table 1. Different operational modes of GRAVICAP for the 3D object trajectory recovery, with the summary of inputs and unknowns. Knowing \vec{u}, B_0, f and \vec{g} allows us to reconstruct B_i .

the operational modes of GRAVICAP and the corresponding sets of unknowns for the object’s trajectory reconstruction.

We solve (2) for B_0, \vec{u} and, optionally, f and \vec{g} by minimising the objective $E_b = E_b(B_0, \vec{u}, f, \vec{g})$ in ℓ_2 -norm:

$$\arg \min_{B_0, \vec{u}, f, \vec{g}} \sum_i \left\| \begin{bmatrix} x_i \\ y_i \end{bmatrix} - \begin{bmatrix} f \frac{X_i}{Z_i} + c_x \\ f \frac{Y_i}{Z_i} + c_y \end{bmatrix} \right\|_2, \quad (4)$$

with X_i, Y_i and Z_i parameterised as in (3). Note that the recovered B_0 and \vec{u} are in absolute units, *i.e.*, m and m/s , since $\|\vec{g}\|$ is expressed in m/s^2 and f (if known) and t are expressed in meters and seconds, respectively.

Remark. From (2), we see that if there is no motion along x - (camera is observing a free fall and the free fall plane is parallel to the image plane) or z - (the free flight plane is parallel to the camera plane) axes, we can still recover the distances in absolute units, since gravity is affecting the y -component of the object’s trajectory only.

While the above formulation (4) is sufficient to recover the object’s trajectory in ideal settings, the accuracy of the estimated trajectory is sensitive to and is often compromised by the observation noise. The sources of this noise can be multiple, including the missing and erroneous centre of gravity detections. We next show how the object’s trajectory and human pose estimation can improve each other.

3.2. Joint 3D Human-Object Reconstruction

Associating the object’s trajectory with the human’s position provides additional constraints while also allowing us to estimate anthropometric information about one or multiple persons in the scene, thanks to the trajectory estimate in the absolute distance units. We first recover unconstrained kinematic estimates of 3D human skeleton $P^{\text{kin}} = \{P_1^{\text{kin}}, P_2^{\text{kin}}, \dots, P_N^{\text{kin}}\}$, where $P_i^{\text{kin}} \in \mathbb{R}^{K \times 3}$ and $K=16$ is the number of joints. We denote individual 3D x -, y - and z -components of each joint, indexed by $k \in \{1, \dots, K\}$, using $P_{i,k,x}^{\text{kin}}, P_{i,k,y}^{\text{kin}}$ and $P_{i,k,z}^{\text{kin}}$, respectively. P^{kin} can be either root-relative or also include an initial estimate of the root translation. In both cases, P^{kin} is estimated separately from the object’s 3D trajectory and, hence, is not provided in absolute coordinates and can be physically implausible.

We use an off-the-shelf 2D pose estimator RMPE (AlphaPose) [10] to extract 2D poses of the person $p = \{p_1, p_2, \dots, p_N\}$, where $p_i \in \mathbb{R}^{K \times 2}$, observed in the input images \mathcal{I} . The root-relative 3D poses P^{kin} of the same person can then be retrieved using an off-the-shelf human pose estimation method like [24, 26, 9]. Those are either lifting methods (*i.e.*, they operate on p) or direct regression approaches operating on \mathcal{I}_i . Since these techniques are monocular (RGB-based), they either predict 3D poses with a canonical skeleton or lack generalisability across different people (body variations).

Our goal is thus to recover the bone lengths, $l = \{l_1, l_2, \dots, l_{K-1}\}$ of the subject, such that the corresponding root-relative 3D poses $s(P^{\text{kin}}, l)$ are in the true metric space and agree with the anatomical lengths. The operator $s(\cdot, \cdot)$ resolves the scale of P^{kin} by rectifying the bone-lengths of P^{kin} with the estimated bone-lengths l , such that the bone direction vectors are preserved. Furthermore, we also estimate the corrective root translations $t^{\text{corr}} = \{t_1^{\text{corr}}, t_2^{\text{corr}}, \dots, t_N^{\text{corr}}\}$ of the person from the camera centre, where $t_i^{\text{corr}} = (t_{i,x}^{\text{corr}}, t_{i,y}^{\text{corr}}, t_{i,z}^{\text{corr}})$. Once the latter are available, the absolute (global) camera-relative pose of the person can be recovered as $P = s(P^{\text{kin}}, l) + t^{\text{corr}}$.

We next assume that in the considered free flight episode, we know when the person is holding the object and when the free flight starts. This allows disambiguating the person’s scale using the recovered trajectory B in the absolute coordinates. Knowing that the object is in contact with the human is necessary. At the moment of contact, the human scale is the same as the trajectory scale (recall that under *scale*, we mean the factor relating the relative and absolute distance units). If there is no contact, the usual ambiguity of the monocular setting along the depth axis still applies to the human and other parts of the scene.

We recover the subject’s poses with respect to the camera by minimising $E_p = E_p(l, t_i^{\text{corr}})$ in ℓ_2 -norm:

$$\arg \min_{l, t^{\text{corr}}} \sum_{i,k} \left\| \begin{bmatrix} p_{i,k}^x \\ p_{i,k}^y \end{bmatrix} - \begin{bmatrix} f \frac{s(P_{i,k}^{\text{kin}}, l)[x] + t_{i,x}^{\text{corr}}}{s(P_{i,k}^{\text{kin}}, l)[z] + t_{i,z}^{\text{corr}}} + c_x \\ f \frac{s(P_{i,k}^{\text{kin}}, l)[y] + t_{i,y}^{\text{corr}}}{s(P_{i,k}^{\text{kin}}, l)[z] + t_{i,z}^{\text{corr}}} + c_y \end{bmatrix} \right\|_2, \quad (5)$$

with operator $\cdot[\bullet]$ extracting x -, y - or z -component of a vector (alternative notation). In (5), we have $2NK$ equations and $(3N+K)$ unknowns for root translations P^r ($3N$ unknowns), bone lengths l ($K-1$ unknowns) and the focal length f . However, the system of equations (5), if considered independently from E_b (4), suffers from scale ambiguity because the bone lengths and root translations counteract each other. Furthermore, pose estimates, both 2D and 3D, are prone to errors due to model inaccuracies; especially, in the case of occlusions. Hence, the estimated object trajectory and the human pose are not guaranteed to be in agreement. It is thus natural to expect reconstructions where the

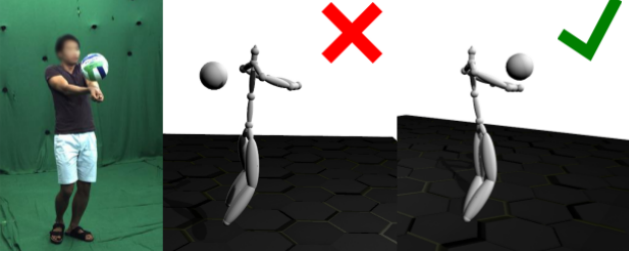


Figure 2. Independently optimising human root translation and object’s trajectory can result in incoherence between the two (middle). We rectify these artefacts by binding human and object positions with contact and mutual localisation constraints.

object’s release position is far away from the point of contact like hands or feet, see Fig. 2. We mitigate these issues in two ways. Firstly, we use a prior on the human bone lengths and impose a symmetry constraint. Secondly, we bind the person’s absolute pose with the object’s trajectory using two additional constraints discussed next.

3.2.1 Constraints on Human Skeleton

The first constraint on the bone lengths $E_{bl}(l)$ ensures that the estimated bone lengths are close the average human bone lengths $\bar{l} = \{\bar{l}_k\}$. For this, we use the average bone lengths collected from the MPI-INF-3DHP [22] dataset:

$$\arg \min_l E_{bl}(l) = \arg \min_l \sum_k^{K-1} \|l_k - \bar{l}_k\|_2^2. \quad (6)$$

Additionally, we ensure that the recovered l are left-right symmetric using the symmetry constraint $E_s(l)$:

$$\arg \min_l E_s(l) = \arg \min_l \sum_{i,j \in \mathcal{S}} \|l_i - l_j\|_2^2, \quad (7)$$

where \mathcal{S} is the set of indices of symmetric bones; E_s corrects asymmetries observed in the initialisations P_i^{kin} , thereby improving the plausibility and accuracy of P_i^{kin} .

3.2.2 Human Contact and Localisation Constraints

The contact term $E_c(P)$ expresses the prior assumption that the object is thrown or caught by the person, *i.e.*, it ensures that the 3D positions of the object and the corresponding body joints at the moment of contact are close to each other:

$$\arg \min_{\vec{u}, \vec{g}, B_0} E_c(P) = \arg \min_{\vec{u}, \vec{g}, B_0} \sum_{(c,t) \in \mathcal{C}} \|P_t^c - B_t\|_2^2, \quad (8)$$

where \mathcal{C} denotes the set of joints in contact with the object at time t , and P_t^c are the 3D coordinates of these joints.

Although (13) binds the object’s trajectory with the human’s absolute position at the points of contact, it does not

explicitly associate the two for the rest of the frames. Also, it does not generalise well to settings where the object is not close to the body at the contact points (*e.g.*, when hitting a ball with a tennis racket).

To address this, we add a *mutual* human-object localisation term E_m to the objective, which ensures that the 3D vectors between the object’s position at frame i and the person’s torso joints—when projected to the image—produce the corresponding observed vectors in the image plane between the object and human joints. This is possible and results in improved 3D human motion capture because the 3D object’s trajectory is smooth and can be estimated highly accurately; we can reliably localise the human with respect to it. For $E_m = E_m(B_0, \vec{u}, f, \vec{g}, l, t^{\text{corr}})$, we choose the torso joints (pelvis, spine, neck, shoulders), because of their stable nature with respect to the camera-relative translation:

$$\arg \min_{B_0, \vec{u}, f, \vec{g}, l, t^{\text{corr}}} \sum_i \sum_{j \in \mathcal{T}} \sum_m^M \left\| \mathbf{d}_{i,j,m}^{2D} - \Pi_f(\mathbf{d}_{i,j,m}^{3D}) \right\|_2^2, \quad (9)$$

$$\text{where } d_{i,j,m}^{2D} = p_{i,j} + \frac{m(b_{i,j} - p_{i,j})}{M}, \text{ and } d_{i,j,m}^{3D} = P_{i,j} + \frac{m(B_{i,j} - P_{i,j})}{M}. \quad (10)$$

where \mathcal{T} is the set of torso joints and $\mathbf{d}_{i,j,m}^{2D}$ and $\mathbf{d}_{i,j,m}^{3D}$ are the vectors between object and torso joint j at frame i in 2D and 3D, respectively. Note that we optimise for 3D vectors guided by their reprojections in the image plane. Such optimisation also influences (in most cases, improves the accuracy of) the corresponding joints j . In practice, we uniformly sample M points in $\mathbf{d}_{i,j}^{2D}$ and $\mathbf{d}_{i,j}^{3D}$, and penalise the projection error. See Fig. 3 for illustration of this principle.

3.2.3 Multi-Episodes and Multi-Person Settings

So far, we have been focusing on a single person and a single episode, *i.e.*, the case of a single ballistic trajectory. We also propose a variant of our method that can handle multi-episodes with consecutive ballistic trajectories and the same person. We assume that f , \vec{g} and the human bone lengths l are constant over the multi-episodes, whereas B_0 and \vec{u} are individual for every episode. To stitch the multiple trajectories coherently, we propose an additional constraint E_{co} , that penalises the differences between the initial object’s position in the current episode and its last position in the previous episode using ℓ_2 -norm.

Furthermore, our method allows for two-person (multi-) episodes (*e.g.*, two persons throwing an object at each other) with minimal changes. To that end, we modify E_p (5) and E_m (9) to account for the projection losses with both persons in the scene. Likewise, the contact loss E_c (13) is altered to account for contacts with different persons at different time instants; see the supplementary material for details.

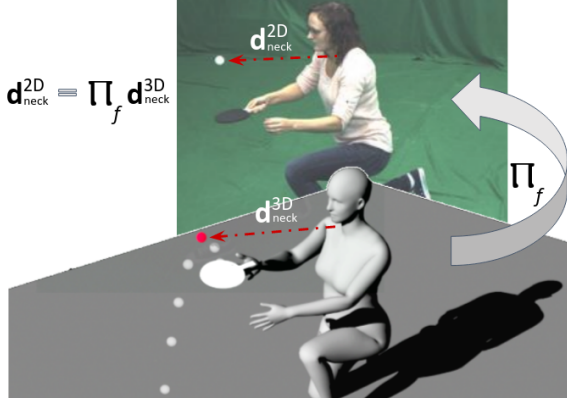


Figure 3. Illustration of the principle behind the human-object localisation term E_m for the neck joint and the second frame of the free flight episode. E_m ensures that the points along the vector connecting the object and the neck joint in 3D (\mathbf{d}_{neck}^{3D}) must project to the corresponding points in the 2D projection of the line (\mathbf{d}_{neck}^{2D}) under perspective projection. In addition to the neck joint, we also use hips, spine and shoulders to compute E_m .

	S1	S2	S3	S4	S5	S6	S7	S8	S9*	Σ
Ball	R	PP	PP	V	V	T	V	T	V	-
L , sec.	8	19	26	14	21	31	21	28	21	193
Σ ME	9	3	6	9	9	12	6	6	3	63
Σ E	12	21	45	18	54	30	30	24	18	252

Table 2. Our dataset contains eight sequences with single subjects (S1–S8) and one sequence with two subjects (S9*). Contents row-wise: (1) Object type, either rubber (R), ping pong (PP), volley (V) or tennis (T) ball; (2) duration L in seconds; (3) number of multi-episodes (ME); (4) number of episodes (E).

3.3. Joint Energy Optimisation

The joint objective term of GRAVICAP can now be expressed as a sum of seven energy terms:

$$E = E_p + \lambda_b E_b + \lambda_c E_c + \lambda_m E_m + \lambda_s E_s + \lambda_{co} E_{co} + \lambda_{bl} E_{bl}, \quad (11)$$

with weights $\lambda_b, \lambda_c, \lambda_m, \lambda_s, \lambda_{bl}$ and λ_{co} balancing the individual terms. As mentioned in Sec. 3.1, GRAVICAP can work in four modes with 6 DoF (\vec{u}, B_0), 7 DoF (\vec{u}, B_0, f), 9 DoF (\vec{u}, B_0, \vec{g}) and 10 DoF (\vec{u}, B_0, \vec{g}, f) for the object’s trajectory.

The total number of unknowns in (11) is $3N+K+9$ for one person and one episode. At the end of this optimisation, our method can reconstruct the object’s absolute 3D trajectory along with the human’s absolute root positions for all the time steps. We solve for the unknowns in (11) using Levenberg-Marquardt [28] with $\lambda_b=1.0, \lambda_p=1.0, \lambda_c=0.1, \lambda_m=0.5, \lambda_{co}=0.1, \lambda_{bl}=0.1$ and $\lambda_s=0.01$. The values of balancing terms are chosen empirically using a hyper-parameter sweep. Note that optimising first (4) disjointly from (11) produced worse results.

3.4. Implementation Details

For every input video, we follow a three-step approach: Retrieving the kinematic human poses P^{kin} , tracking the 2D object’s trajectory \mathbf{b} , and finally, minimising (11).

Estimating Human Poses. We estimate the initial 3D positions of human skeleton joints using the real-time VNect method [24] for the single-person case and XNect [23] for the multi-person setting. These methods provide absolute 3D positions in camera coordinates which serve as a reasonable initialisation for GRAVICAP. For 2D joint positions, we use AlphaPose [10]. To accommodate a differing number of joints across methods, we consider the skeleton structure of MPII 2D pose dataset [1] with $K=16$ joints.

Object Tracking Method. The object tracklets are retrieved using OpenCV’s off-the-shelf CSR Tracker [20]. For initialising the tracker, we localise the object in the first frame by performing template matching with a reference image. If an object detector exists for the target object (e.g., basketball), we recommend using it for the localisation. For the multi-episode setting, we detect the switch of episodes based on the sudden change of the object’s 2D velocity direction. Since this change also happens during the movement along the ballistic trajectory (though much slower), we use a threshold on the velocity direction to distinguish the episodes (cf. our supplement).

4. Dataset for 3D Human-Object Recovery

To evaluate the performance of our approach and establish an evaluation benchmark for future works, we record a new dataset with four subjects performing a variety of activities with four ball types. The dataset includes eight sequences with a single person and one additional sequence with two persons. For each sequence, we provide three synchronised videos of the scene, ground-truth intrinsic and extrinsic camera parameters, ground-truth human poses (both 2D, for each view, and 3D) and ground-truth object trajectories (both 2D, for each view, and 3D). For tracking 3D human joints, we use multi-view a markerless motion capture system [5] with 101 camera views. Ground-truth object trajectories are recovered using triangulation. Each sequence contains several multi-episodes, i.e., consecutive sets of observed free flights. See Table 2 for the summary.

5. Experiments

To demonstrate the quality of the estimated 3D motions, we compare our results with existing state-of-the-art methods that estimate human poses in camera-relative space: VNect [24], MotioNet [37] and PhysCap [39]. Additionally, we include a recent method VIBE [17] for root-relative pose estimation, which currently achieves state-of-the-art accuracy in this category. Note that VIBE is not a competing method since it cannot estimate global root translations.

		S1	S2	S3	S4	S5	S6	S7	S8	Avg
global root positions, MPE [mm] ↓	PhysCap [39]	431.1	225.6	232.3	239.2	223.1	446.5	358.8	420.28	309.7
	VNect [24]	413.3	136.6	239.8	175.0	153.9	354.4	324.0	438.0	262.0
	Ours (10 DoF)	219.7	111.3	234.8	166.9	157.4	332.1	187.7	377.4	224.5
	Ours (9 DoF)	411.9	132.3	232.7	118.9	157.6	149.9	135.7	352.4	191.3
root-relative poses, MPJPE [mm] ↓	PhysCap [39]	126.3	128.6	94.8	129.1	116.9	138.4	148.8	131.9	125.2
	VIBE [17]	126.4	114	104.81	99.3	105.3	126.9	132.05	105.3	113.2
	VNect [24]	127.7	131.0	125.33	150.2	128.6	134.4	143.8	140.8	134.0
	Ours (10 DoF)	120.7	119.6	109.9	130.8	120.03	126.3	140.4	134.6	124.4
	Ours (9 DoF)	119.2	127.6	108.9	144.7	113.1	125.8	130.7	131.2	122.8
bone lengths (l), MAE [mm] ↓	VNect[24]	71.4	63	83.7	79.0	79.9	80.3	76.3	83.8	78.4
	Ours (10 DoF)	64.0	52.6	62.2	60.7	61.8	58.5	84.4	64.6	63.3
	Ours (9 DoF)	64.3	48.3	65.1	64.8	59.5	65.8	60.2	65.1	61.1
3D object positions (B_i), MPE [mm] ↓	10 DoF	451.0	309.0	760.3	304.0	476.8	372.3	280.6	470.7	445.5
	9 DoF	396.4	509.0	749.3	310.9	509.3	463.7	229.1	493.6	482.9
gravity direction (\vec{g}), cosine similarity ↑	10 DoF	0.927	0.977	0.954	0.949	0.99	0.99	0.951	0.975	0.972
	9 DoF	0.923	0.959	0.956	0.972	0.984	0.985	0.977	0.970	0.972

Table 3. Comparisons of various 3D errors on the new dataset (Sec. 4) with human-object interactions. Note that VIBE [17] outputs root-relative poses only and, hence, cannot compete in global estimations. The **bold/italicised bold** font denotes the best/second-best number. The last column provides the frame-weighted averages per sequence. ‘↓’(‘↑’) stands for ‘the lower (the higher) the better’.

The pre-trained models that the authors provide are used for the comparisons. We report the root-relative Mean Per Joint Position Error (MPJPE), the Mean Position Error (MPE) of the camera-relative root translation, as well as smoothness error of the estimated 3D poses [39]. We also evaluate the accuracy of the ground plane orientation estimation and report the cosine similarity between the ground-truth and estimated gravity direction vectors. Since GRAVICAP also estimates bone lengths, we report Mean Absolute Error (MAE), *i.e.*, mean of the per-bone absolute differences between the ground-truth and predicted lengths. We also report the estimated heights of subjects from the new dataset. Finally, we evaluate the accuracy of the object’s trajectory using MPE.

All experiments are performed on a system with 32GB RAM and AMD Ryzen ThreadRipper CPU, under operating system Ubuntu 18.04. The method is implemented in SciPy [43]. The runtime of the optimisation depends on the number of episodes in the sequence and ranges from three seconds for a single episode to roughly five minutes for a multi-episode with twelve trajectories.

5.1. Quantitative Results

Table 3 summarises the comparisons of 3D human motion capture. 9 DoF refers to the setting in which B_0 , \vec{u} and \vec{g} are unknown. In the experiments with 10 DoF, focal length f is also unknown (however, VNect uses the ground-truth f), *cf.* Table 1 with the summary of operational modes. We observe significant improvements in global root translation estimation over VNect [24] and PhysCap [39], *i.e.*, we outperform both methods in seven cases out of eight. Note that MotioNet [37] is not able to produce reasonable estimates, and we do not include it in Table 3. All tested algo-

gorithms show MPJPE for root-relative 3D joint positions in the comparable ranges. While VIBE [17] shows the lowest error for the root-relative poses overall, it cannot estimate global root translations. Note that only our method additionally estimates the floor normal, whereas other methods either require it as input or are agnostic to it. Fig. 4 provides a few visualisations of the results obtained by GRAVICAP.

In bone length estimation, GRAVICAP outperforms VNect in all cases. Note that VNect and PhysCap implicitly assume a known average human height of a pre-defined skeleton. The second-lowest row block of Table 3 summarises the accuracy of the 3D object’s trajectories estimation (only our method can estimate those; the numbers are provided for future reference). GRAVICAP can also estimate gravity directions. This is advantageous since we can obtain the floor normal, assuming that the gravity vector is perpendicular to the ground plane. We report cosine similarity between the ground-truth gravity direction and the estimated one in Table 3 (the lowest row block). As can be seen, our algorithm estimates highly accurate gravity direction given only a monocular video.

3D MPJPE considered in isolation can hide artefacts in the reconstructed motions such as jitters, which has been recently demonstrated [39]. Smoothness in motions is thus an important criterion of physical plausibility. Therefore, we report smoothness error e_{smooth} proposed in [39] in Table 4. Our algorithm outperforms VNect and VIBE on this metric, thanks to mutual localisation term (9) and stable bone length estimation. PhysCap performs best because of the explicit physics model and the assumption of known body mass distribution and subject’s height, unlike our method.

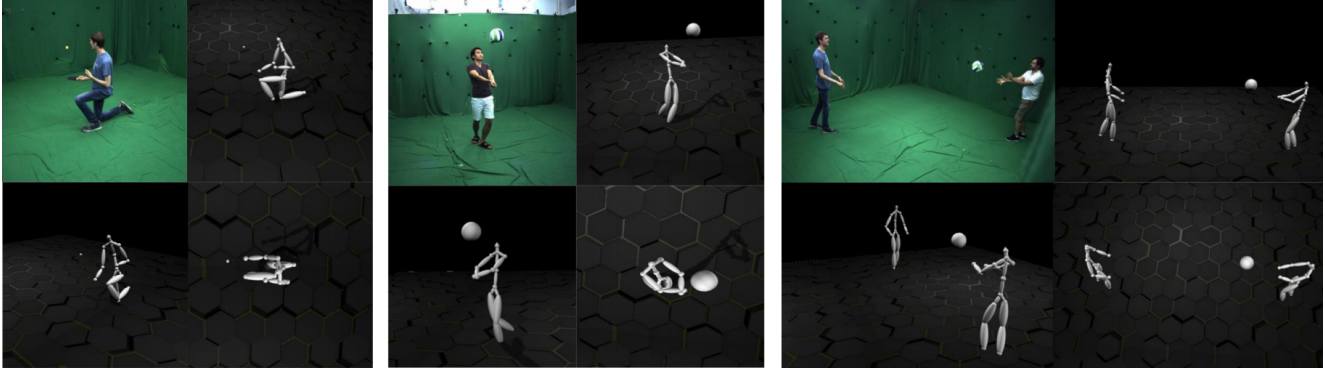


Figure 4. 3D human-object reconstructions of GRAVICAP (from left to right: S2, S4 and S9). In each image set out of three, we show the input view (top-left) and our reconstructions from three arbitrary views in 3D. See the supplementary video for the dynamic visualisations.

Human Height Estimation. We recover the subjects’ heights from the estimated scale and root translations. We first calculate the head-toe distance h_{px} in the image with the subject in the upright pose using AlphaPose [10, 3]. Since AlphaPose estimates only the head centre and ankles instead of head-top and feet/heels, we scale up the estimated height with a factor of 1.17, as suggested in Bieler *et al.* [3]. Finally, we compute the actual height of the person as $h_{3d} = \frac{t_z^{corr}}{f} h_{px}$. We observe an average height error of 6.75 cm across all four subjects of the new dataset.

	Ours	VNect [24]	VIBE [17]	PhysCap* [39]
e_{smooth}	10.74	11.35	11.32	7.72

Table 4. Comparisons using e_{smooth} . We reduce the jitter compared to VNect owing to the mutual-direction constraint and more accurate bone-length estimation. ‘*’ indicates the assumption of known body mass distribution and ground plane orientation.

5.2. In-the-Wild Experiments

In addition to the quantitative analysis on the new dataset, we test our method on in-the-wild settings (*e.g.*, practising basketball and shot put); see our supplement.

6. Discussion and Limitations

Joint 3D human motion capture and 3D trajectory reconstruction of objects in free flights is a new problem in computer vision. Our core method addresses it without relying on 3D training data; a learning-based approach is used only to initialise human poses. Yet, GRAVICAP performs close to the state-of-the-art learning-based methods for root-relative human pose estimation [17], when compared in the accuracy of root-relative poses. Regarding absolute poses, we significantly outperform 3D motion capture methods estimating camera-relative root translations [24, 39, 26]. At the same time, our estimates of absolute bone lengths are

the most accurate among all methods (if we assume average human height to convert normalised outputs to metric values for the competing techniques).

Note that we use VNect for the initialisation, which is not state-of-the-art. This shows that the final superior accuracy is reached thanks to the proposed energy terms and awareness of the law of gravitation. In the absence of camera intrinsics, we either need well-initialised absolute root translations, or we can only estimate the scene’s scale in most cases, due to the ‘ f/Z ’ ambiguity in (2). Although the system is largely automatic, our framework strongly relies on the object’s bounding box in the first frame and the hand-object contact joint detections, which can be difficult to obtain without specialised methods (see Sec. 3.4).

To be applied on the Moon or Mars, GRAVICAP would require the corresponding local $\|\vec{g}\|$. Our method assumes, per default, that humans hold objects in their hands. If this assumption is not fulfilled, it requires a prior on the type of the used instrument which propagates forces exerted by the human. Furthermore, since GRAVICAP is a lifting approach, its accuracy depends on 2D human poses and 2D object detections, similar to several other monocular 3D human motion capture methods [24, 39].

7. Conclusion

We introduced GRAVICAP and showed experimentally that given only a monocular video, in which humans interact with objects and bring them to free flights, it is possible to recover distances in meters (bone lengths and camera’s focal length), the orientation of the ground plane relative to the camera, as well as significantly improve the initial kinematic human pose estimates reaching state-of-the-art accuracy. This changes the way how we think about the young subfield of joint 3D human-object reconstruction and opens up many avenues for future research.

Acknowledgements. This work was supported by the ERC consolidator grant 4DReply (770784).

References

- [1] Mykhaylo Andriluka, Leonid Pishchulin, Peter Gehler, and Bernt Schiele. 2d human pose estimation: New benchmark and state of the art analysis. In *Computer Vision and Pattern Recognition (CVPR)*, 2014. 6
- [2] Kiran S. Bhat, Steven M. Seitz, Jovan Popović, and Pradeep K. Khosla. Computing the physical parameters of rigid-body motion from video. In *European Conference on Computer Vision (ECCV)*, pages 551–565, 2002. 3
- [3] Didier Bieler, Semih Gunel, Pascal Fua, and Helge Rhodin. Gravity as a reference for estimating a person’s height from video. In *International Conference on Computer Vision (ICCV)*, 2019. 3, 8
- [4] Federica Bogo, Angjoo Kanazawa, Christoph Lassner, Peter Gehler, Javier Romero, and Michael J. Black. Keep it SMPL: Automatic estimation of 3D human pose and shape from a single image. In *European Conference on Computer Vision (ECCV)*, 2016. 2
- [5] The Captury. <http://www.thecaptury.com/>. 6
- [6] Ching-Hang Chen and Deva Ramanan. 3d human pose estimation = 2d pose estimation + matching. In *Computer Vision and Pattern Recognition (CVPR)*, 2017. 2
- [7] Ching-Hang Chen, Amrith Tyagi, Amit Agrawal, Dylan Drover, Rohith MV, Stefan Stojanov, and James M. Rehg. Unsupervised 3d pose estimation with geometric self-supervision. In *Computer Vision and Pattern Recognition (CVPR)*, 2019. 2
- [8] Rishabh Dabral, Nitesh B Gundavarapu, Abhishek Mitra, Rahuland Sharma, Ganesh Ramakrishnan, and Arjun Jain. Multi-person 3d human pose estimation from monocular images. In *International Conference on 3D Vision (3DV)*, 2019. 2
- [9] Rishabh Dabral, Anurag Mundhada, Uday Kusupati, Safer Afaque, Abhishek Sharma, and Arjun Jain. Learning 3d human pose from structure and motion. In *European Conference on Computer Vision (ECCV)*, 2018. 2, 4
- [10] Hao-Shu Fang, Shuqin Xie, Yu-Wing Tai, and Cewu Lu. RMPE: Regional multi-person pose estimation. 2017. 4, 6, 8
- [11] Hao-Shu Fang, Yuanlu Xu, Wenguan Wang, Xiaobai Liu, and Song-Chun Zhu. Learning pose grammar to encode human body configuration for 3d pose estimation. In *AAAI Conference on Artificial Intelligence*, 2018. 2
- [12] Marc Habermann, Weipeng Xu, Michael Zollhoefer, Gerard Pons-Moll, and Christian Theobalt. Deepcap: Monocular human performance capture using weak supervision. In *Computer Vision and Pattern Recognition (CVPR)*, 2020. 2
- [13] Marc Habermann, Weipeng Xu, Michael Zollhoefer, Gerard Pons-Moll, and Christian Theobalt. Livecap: Real-time human performance capture from monocular video. *ACM Transactions On Graphics (TOG)*, 38(2):14:1–14:17, 2019. 2
- [14] Ikhsanul Habibie, Weipeng Xu, Dushyant Mehta, Gerard Pons-Moll, and Christian Theobalt. In the wild human pose estimation using explicit 2d features and intermediate 3d representations. In *Computer Vision and Pattern Recognition (CVPR)*, 2019. 1, 2
- [15] Mohamed Hassan, Vasileios Choutas, Dimitrios Tzionas, and Michael J. Black. Resolving 3D human pose ambiguities with 3D scene constraints. In *International Conference on Computer Vision (ICCV)*, 2019. 1, 2
- [16] Angjoo Kanazawa, Michael J. Black, David W. Jacobs, and Jitendra Malik. End-to-end recovery of human shape and pose. In *Computer Vision and Pattern Recognition (CVPR)*, 2018. 2
- [17] Muhammed Kocabas, Nikos Athanasiou, and Michael J. Black. Vibe: Video inference for human body pose and shape estimation. In *Computer Vision and Pattern Recognition (CVPR)*, 2020. 2, 6, 7, 8
- [18] Onorina Kovalenko, Vladislav Golyanik, Jameel Malik, Ahmed Elhayek, and Didier Stricker. Structure from articulated motion: Accurate and stable monocular 3d reconstruction without training data. *Sensors*, 19(20), 2019. 2
- [19] Zongmian Li, Jiri Sedlar, Justin Carpentier, Ivan Laptev, Nicolas Mansard, and Josef Sivic. Estimating 3d motion and forces of person-object interactions from monocular video. In *Computer Vision and Pattern Recognition (CVPR)*, 2019. 1, 2
- [20] Alan Lukežič, Tomáš Vojtíš, Luka Čehovin Zajc, Jiří Matas, and Matej Kristan. Discriminative correlation filter with channel and spatial reliability. In *Computer Vision and Pattern Recognition (CVPR)*, 2017. 6
- [21] Julieta Martinez, Rayat Hossain, Javier Romero, and James J. Little. A simple yet effective baseline for 3d human pose estimation. In *International Conference on Computer Vision (ICCV)*, 2017. 1, 2
- [22] Dushyant Mehta, Helge Rhodin, Dan Casas, Pascal Fua, Oleksandr Sotnychenko, Weipeng Xu, and Christian Theobalt. Monocular 3d human pose estimation in the wild using improved cnn supervision. In *International Conference on 3D Vision (3DV)*, 2017. 2, 5
- [23] Dushyant Mehta, Oleksandr Sotnychenko, Franziska Mueller, Weipeng Xu, Mohammad Elgharib, Hans-Peter Seidel, Helge Rhodin, Gerard Pons-Moll, and Christian Theobalt. Xnect: Real-time multi-person 3d motion capture with a single rgb camera. *ACM Transactions on Graphics (TOG)*, 2020. 2, 6
- [24] Dushyant Mehta, Srinath Sridhar, Oleksandr Sotnychenko, Helge Rhodin, Mohammad Shafiei, Hans-Peter Seidel, Weipeng Xu, Dan Casas, and Christian Theobalt. Vnect: Real-time 3d human pose estimation with a single rgb camera. *ACM Transactions on Graphics*, 2017. 1, 2, 4, 6, 7, 8
- [25] Aron Monszpart, Paul Guerrero, Duygu Ceylan, Ersin Yumer, and Niloy J. Mitra. iMapper: Interaction-guided scene mapping from monocular videos. *ACM SIGGRAPH*, 2019. 2
- [26] Gyeongsik Moon, Juyong Chang, and Kyoung Mu Lee. Camera distance-aware top-down approach for 3d multi-person pose estimation from a single rgb image. In *International Conference on Computer Vision (ICCV)*, 2019. 2, 4, 8
- [27] Francesc Moreno-Noguer. 3d human pose estimation from a single image via distance matrix regression. In *Computer Vision and Pattern Recognition (CVPR)*, 2017. 2

- [28] Jorge J. Moré. The levenberg-marquardt algorithm: Implementation and theory. In *Numerical Analysis*. 1978. 6
- [29] Alejandro Newell, Kaiyu Yang, and Jia Deng. Stacked hourglass networks for human pose estimation. In *European Conference on Computer Vision (ECCV)*, 2016. 2
- [30] David Novotny, Nikhila Ravi, Benjamin Graham, Natalia Neverova, and Andrea Vedaldi. C3dpo: Canonical 3d pose networks for non-rigid structure from motion. In *International Conference on Computer Vision (ICCV)*, 2019. 2
- [31] Georgios Pavlakos, XiaoWei Zhou, Konstantinos G. Derpanis, and Kostas Daniilidis. Coarse-to-fine volumetric prediction for single-image 3d human pose. In *Computer Vision and Pattern Recognition (CVPR)*, 2017. 2
- [32] Georgios Pavlakos, Luyang Zhu, XiaoWei Zhou, and Kostas Daniilidis. Learning to estimate 3d human pose and shape from a single color image. In *Computer Vision and Pattern Recognition (CVPR)*, 2018. 2
- [33] Dario Pavlo, Christoph Feichtenhofer, David Grangier, and Michael Auli. 3d human pose estimation in video with temporal convolutions and semi-supervised training. In *Computer Vision and Pattern Recognition (CVPR)*, 2019. 1
- [34] Davis Remppe, Leonidas J Guibas, Aaron Hertzmann, Bryan Russell, Ruben Villegas, and Jimei Yang. Contact and human dynamics from monocular video. In *European Conference on Computer Vision (ECCV)*, 2020. 1, 3
- [35] Helge Rhodin, Mathieu Salzmann, and Pascal Fua. Unsupervised geometry-aware representation learning for 3d human pose estimation. In *European Conference on Computer Vision (ECCV)*, 2018. 2
- [36] Grégory Rogez, Philippe Weinzaepfel, and Cordelia Schmid. LCR-Net++: Multi-Person 2D and 3D Pose Detection in Natural Images. *Transactions on Pattern Analysis and Machine Intelligence (TPAMI)*, 2019. 2
- [37] Mingyi Shi, Kfir Aberman, Andreas Aristidou, Taku Komura, Dani Lischinski, Daniel Cohen-Or, and Baoquan Chen. Motionet: 3d human motion reconstruction from monocular video with skeleton consistency. *ACM Transactions on Graphics (TOG)*, 2020. 2, 6, 7
- [38] Soshi Shimada, Vladislav Golyanik, Weipeng Xu, Patrick Pérez, and Christian Theobalt. Neural monocular 3d human motion capture with physical awareness. *ACM Transactions on Graphics*, 40(4), 2021. 3
- [39] Soshi Shimada, Vladislav Golyanik, Weipeng Xu, and Christian Theobalt. Physcap: physically plausible monocular 3d motion capture in real time. *ACM Transactions on Graphics (TOG)*, 39(6), 2020. 1, 3, 6, 7, 8
- [40] Bugra Tekin, Isinsu Katircioglu, Mathieu Salzmann, Vincent Lepetit, and Pascal Fua. Structured prediction of 3d human pose with deep neural networks. In *British Machine Vision Conference (BMVC)*, 2016. 2
- [41] Denis Tomè, Chris Russell, and Lourdes Agapito. Lifting from the deep: Convolutional 3d pose estimation from a single image. In *Computer Vision and Pattern Recognition (CVPR)*, 2017. 2
- [42] Aggeliki Tsoli, Matthew Loper, and Michael J. Black. Model-based anthropometry: Predicting measurements from 3d human scans in multiple poses. In *Winter Conference on Applications of Computer Vision (WACV)*, 2014. 3
- [43] Pauli Virtanen, Ralf Gommers, Travis E. Oliphant, Matt Haberland, Tyler Reddy, David Cournapeau, Evgeni Burovski, Pearu Peterson, Warren Weckesser, Jonathan Bright, Stéfan J. van der Walt, Matthew Brett, Joshua Wilson, K. Jarrod Millman, Nikolay Mayorov, Andrew R. J. Nelson, Eric Jones, Robert Kern, Eric Larson, C J Carey, İlhan Polat, Yu Feng, Eric W. Moore, Jake VanderPlas, Denis Laxalde, Josef Perktold, Robert Cimrman, Ian Henriksen, E. A. Quintero, Charles R. Harris, Anne M. Archibald, Antônio H. Ribeiro, Fabian Pedregosa, Paul van Mulbregt, and SciPy 1.0 Contributors. SciPy 1.0: Fundamental Algorithms for Scientific Computing in Python. *Nature Methods*, 17:261–272, 2020. 7
- [44] Marek Vondrak, Leonid Sigal, Jessica Hodgins, and Odest Jenkins. Video-based 3d motion capture through biped control. *ACM Transactions On Graphics (TOG)*, 31(4), 2012. 2
- [45] Bastian Wandt, Hanno Ackermann, and Bodo Rosenhahn. 3d reconstruction of human motion from monocular image sequences. *Transactions on Pattern Analysis and Machine Intelligence (TPAMI)*, 38(8):1505–1516, 2016. 2
- [46] Bastian Wandt and Bodo Rosenhahn. Repnet: Weakly supervised training of an adversarial reprojection network for 3d human pose estimation. In *Computer Vision and Pattern Recognition (CVPR)*, 2019. 2
- [47] Oliver Wasenmüller, Jan C. Peters, Vladislav Golyanik, and Didier Stricker. Precise and automatic anthropometric measurement extraction using template registration. In *International Conference on 3D Body Scanning Technologies (3DBODYTECH)*, 2015. 3
- [48] Lan Xu, Weipeng Xu, Vladislav Golyanik, Marc Habermann, Lu Fang, and Christian Theobalt. Eventcap: Monocular 3d capture of high-speed human motions using an event camera. In *Computer Vision and Pattern Recognition (CVPR)*, 2020. 2
- [49] Andrei Zanfir, Elisabeta Marinoiu, and Cristian Sminchisescu. Monocular 3d pose and shape estimation of multiple people in natural scenes - the importance of multiple scene constraints. In *Computer Vision and Pattern Recognition (CVPR)*, 2018. 1, 2
- [50] Jason Y. Zhang, Sam Pepose, Hanbyul Joo, Deva Ramanan, Jitendra Malik, and Angjoo Kanazawa. Perceiving 3d human-object spatial arrangements from a single image in the wild. In *European Conference on Computer Vision (ECCV)*, 2020. 1, 2
- [51] XiaoWei Zhou, Spyridon Leonardos, Xiaoyan Hu, and Kostas Daniilidis. 3d shape estimation from 2d landmarks: A convex relaxation approach. In *Computer Vision and Pattern Recognition (CVPR)*, 2015. 2

Supplementary Material

This supplementary material contains further details on GRAVICAP. We also provide a supplementary video with further analysis of our method, in-the-wild 3D reconstructions and qualitative comparisons with other methods.

A. In-the-Wild Results

To verify the accuracy of visual metrology achievable by our method, we test it on several real-world scenarios where the distance references are available.



Figure 5. Shot put sequence

Professional Shotput Throw: A professional shot put thrower can throw in the range of 20 meters. The image in Fig. 5 is a reference to a throw by the world record holder Ryan Crouser². Since the person is extremely blurred in the clip, we test our method with only object-related constraint E_b , while ensuring that the magnitude of gravity vector is 9.81 m/s^2 . Our method estimates the throw to be 18.557 m long. Further, we estimate the maximum point of the object’s trajectory to be 5.46 m . Finally, the estimated gravity direction indicates an upward tilt of 13° of the camera.

Basketball Throw: We measure the final position of the ball in the trajectory of the throw depicted in Fig. 6. We note the absolute y -position of the ball when it touches the hoop and compare it with the absolute y -position of the feet (as estimated by VNect). The difference between the two gives us an estimate of the height of the hoop. The trajectory estimates show a height of 3.03 m , which is close to the actual height of the hoop (3.05 m).

	GT	$\sigma = 10$	$\sigma = 30$	$\sigma = 50$	$\sigma = 100$
Pose, 6 DoF	11.7	23.2	39.9	88.3	227.2
Pose, 7 DoF	8.9	13.4	31.1	69.8	224
Pose, 10 DoF	26.3	60.87	126.5	150.4	225.0
Object	12.4	76.3	134.4	155.8	>400

Table 5. Comparing the effect of adding Gaussian noise to the ground-truth 3D poses and 2D object trajectories on root translation predictions. The unit of σ is mm for poses and pixels for 2D object trajectories.

B. Noise Sensitivity Analysis

To test the sensitivity of GRAVICAP to noise, we perform a sensitivity analysis and summarise the results in Table 5. As expected, the performance is affected by strong 2D object trajectory perturbations, as high σ , *i.e.*, the standard deviation of Gaussian noise, disrupts its parabolic nature.

²<https://www.youtube.com/watch?v=TZANFlvsXv4>



Figure 6. Basketball throw sequence from <https://www.youtube.com/watch?v=BKIOqbx3sbU>.

C. Detection of Trajectory Breaks

To detect an episode switch in multi-episode sequences, we traverse the 2D trajectory with a sliding window of five frames. During each slide, we measure the position difference between the positions of the objects in adjacent frames. For a switch to have occurred, the direction of position differences of the first half must be opposite to that of the second half. This, however, is not sufficient for detecting a switch, as the same happens when the object reaches its peak. To confirm a switch, we measure the change in magnitude of velocity during the inversion. We set a threshold of 10 pixels per frame to confirm the episode switch.

D. Handling Multi-Episodes and Two Persons

Multi-Episodes: Whenever we have a multi-episode sequence, we perform joint optimisation on all the episodes. This leads to coherent reconstruction in the sense that the trajectory is continuous and jitter-free. For this, we impose the continuity constraint, E_{co} , that ensures that the last position of the previous episode is the same as the first position of the current episode. Specifically, if $i = 2, 3, \dots$ refers to an episode in a multi-episode sequence, then

$$\arg \min_{\vec{u}, \vec{g}, B_0} E_{co} = \arg \min_{\vec{u}, \vec{g}, B_0} \left\| B_T^{i-1} - B_0^i \right\|_2^2, \quad (12)$$

where T is the number of frames in the i^{th} episode.

Two Persons: For the case with two persons, while the pose projection constraint remains the same (only this time, applied to multiple poses), the contact term needs to accommodate information about which person the object is in contact with:

$$\arg \min_{\vec{u}, \vec{g}, B_0} E_c(P) = \arg \min_{\vec{u}, \vec{g}, B_0} \sum_{(c,t) \in \mathcal{C}} \left\| P_t^{c,\delta} - B_t \right\|_2^2. \quad (13)$$

In this equation, $P_t^{c,\delta}$ indicates the 3D position of the joint c of the person δ ($|\delta|$ is the number of people in the scene) at time of contact t .

E. Dataset Structure

Our dataset consists of nine activity sequences (eight single-person and one with two persons) performed by four subjects. For

```
Root
|- S1
  |- Cam1
    |- Eps1
      annot_e1.pkl
      |- Images
        s_01_c_01_e_01_00001.jpg
        s_01_c_01_e_01_00002.jpg
        ...
    |- Eps2
      annot_e2.pkl
      |- Images
        s_01_c_01_e_02_00001.jpg
        s_01_c_01_e_02_00002.jpg
        ...
```

Figure 7. Dataset structure tree

each sequence, we have two-three multi-episodes involving one or more episodes in succession. We provide annotations and images for up to three camera views. The annotations include the 2D and 3D human poses, 2D and 3D object trajectories, the camera calibration parameters and point-of-contact information (frame numbers and joints which are closest to the body at the time of contact). The images are of size 1200x877 px. The structure of the dataset is demonstrated in Fig. 7.